

Missing Gamma-Rays from kpc-scale AGN Jets: A Test of the IC/CMB Model

Eileen T. Meyer

Space Telescope Science Institute, Baltimore, MD 21218, USA and
University of Maryland Baltimore County, Baltimore, MD 21250, USA

Markos Georganopoulos

University of Maryland Baltimore County, Baltimore, MD 21250, USA

W. B. Sparks

Space Telescope Science Institute, Baltimore, MD 21218, USA

Leith Godfrey

ASTRON Netherlands Institute for Radio Astronomy, The Netherlands

Eric Perlman

Florida Institute of Technology, Melbourne, FL 32901, USA

The physical origin of the X-ray emission in powerful quasar jets has been a long-standing mystery. Though these jets start out on the sub-pc scale as highly relativistic flows, we do not have any direct measurement of their speeds on the kpc scale, where the vast distances from the core necessitate in situ particle acceleration. If the jets remain highly relativistic on kpc scales, then the X-rays could be due to inverse-Compton upscattering of CMB photons. However, the IC/CMB explanation predicts a high level of gamma-ray emission, which should be detectable by the *Fermi*/LAT. We have searched for and ruled out this emission at a high level of significance for the well-known sources 3C 273 and PKS 0637-752, suggesting the X-rays are synchrotron, though of unknown origin. These recent results with *Fermi* also suggest that the kpc-scale jets in powerful quasars are significantly slower than have been presumed under the IC/CMB model. I will discuss the surprising implications of these findings for the energetics and radiative output of powerful quasars as well as their impact on their environment.

In August 1999, the *Chandra* X-ray Observatory observed its first celestial target, quasar PKS 0637-752, during the initial focusing of the telescope [Schwartz et al. 2000, Chartas et al. 2000]. Along with the bright quasar core, *Chandra* unexpectedly detected X-rays from the kilo-parsec scale relativistic jet (previously known from radio imaging, Figure). Unlike the synchrotron spectrum of lower-power FR I jets like M87 which easily extend up to X-ray energies [e.g. Wilson and Yang 2002], the synchrotron spectrum of powerful quasar jets (including PKS 0637-752) generally peak at or below the IR/Optical band. The X-rays detected in the kpc-scale jet of PKS 0637-752 were orders of magnitude brighter than expected from the radio-optical synchrotron spectrum, or indeed from either synchrotron self-Compton (SSC) or inverse Compton upscattering of ambient CMB photons (IC/CMB) under equipartition conditions [Chartas et al. 2000]. Further, the X-ray spectrum of the jet was remarkably hard, with a photon index of 1.76 ± 0.1 .

Proper motions measurements of sub-parsec scale jets of powerful quasars with Very Long Baseline Interferometry (VLBI) have detected superluminal proper motions which imply that these jets start out highly relativistic, with Lorentz factors (Γ) of 10-50 [Jorstad et al. 2005, Lister et al. 2009]. Though it had long been supposed based on population studies that jets decelerate and are at most mildly relativistic by the time they reach the kpc scale [e.g. Arshakian and Longair 2004, Mullin and Hardcastle

2009], no direct measurements have confirmed this. Tavecchio et al. [2000] and Celotti et al. [2001] thus suggested that the X-rays from the jet in PKS 0637-752 could be explained by IC/CMB emission if the jet *remained* highly relativistic ($\Gamma \sim 10$), and was pointed at a fairly small angle to our line of sight (6°). This produces a much larger Doppler boosting factor ($\delta \sim 10$) and enables the IC/CMB X-rays to match the observations.

Over the past decade and a half since the launch of *Chandra*, dozens more kpc-scale quasar jets with anomalously hard and/or high X-rays have been detected [e.g. Sambruna et al. 2001, 2002, Siemiginowska et al. 2003, Sambruna et al. 2004, Marshall et al. 2005, Harris and Krawczynski 2006, Siemiginowska et al. 2007, Marshall et al. 2011, Kharb et al. 2012, Godfrey et al. 2012]. The IC/CMB model has been by far the most popular explanation of these X-rays, though problems have been noted [Hardcastle 2006]. Besides the unconfirmed fast speeds required on the kpc scale, IC/CMB often requires the jet to be pointed very close along our line-of-sight, leading to a deprojected jet length longer than 1 Mpc, the upper limit for jets observed in the plane of the sky. Further, the electrons responsible for upscattering the CMB into the *Chandra* band are at much lower energies than are traced by radio observations. This extension of the electron energy distribution is energetically costly, in some cases leading to ‘super-Eddington’ jet power requirements [Dermer and Atoyan 2004,

Uchiyama et al. 2006]. These problems lead to the suggestion that the X-rays could alternatively be synchrotron emission from a second electron population in the jet, albeit of unknown origin [Hardcastle 2006, Uchiyama et al. 2006, Jester et al. 2006, Harris et al. 2004, Kataoka and Stawarz 2005]. The fundamental problem up to now has been that fitting the radio-to-X-ray spectral energy distribution (SED) alone cannot distinguish between the IC/CMB and synchrotron explanations for the X-rays [Cara et al. 2013]. The difference in power requirements between the two mechanisms is great, as is the extremely different idea of jet structure that they imply. Discriminating between these models is essential to make progress on the actual impact of jets on their environment.

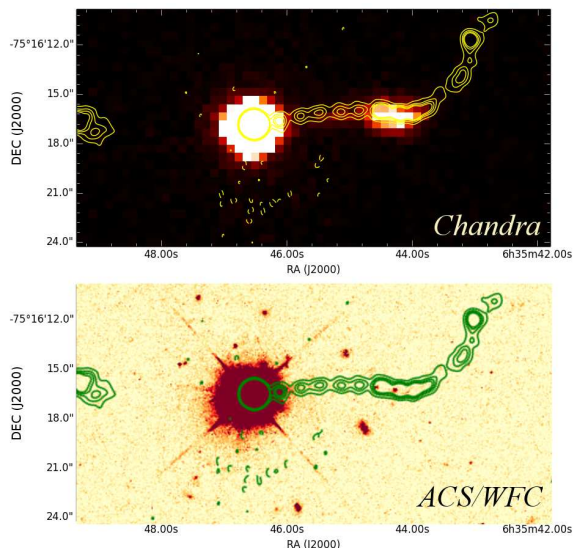


Figure 1: *Upper Panel:* *Chandra* X-ray image of PKS 0637-752, with ATCA 17 GHz radio contours overlaid. *Lower Panel:* Optical image of PKS 0637-752, taken with ACS/WFC on HST (F475W filter) with ATCA 17 GHz radio contours overlaid.

Georganopoulos et al. [2006], hereafter **G06**, suggested that *Fermi* Large Area Telescope (LAT) observations could confirm or rule out the IC/CMB mechanism for the X-rays, by detecting (or not) the high level of gamma-ray emission this mechanism requires. We have previously looked for this gamma-ray emission from the jet of 3C 273, and ruled out IC/CMB gamma-rays from (the brightest) knot A alone at the >95% level, and from knots A through D1 combined at the >99.9% level [Meyer and Georganopoulos 2014, hereafter **M14**].

At this meeting, we reported new *Fermi* observations of PKS 0637-752 which show that the expected steady gamma-ray emission from the IC/CMB mechanism is also ruled out by deep upper limits at the 99.9% level. We also present updated limits for 3C 273, showing that the expected gamma-rays from

IC/CMB are now ruled out at the 99.99% level in more than one *Fermi* energy band. We will briefly discuss the implications of these measurements on two fronts. First, we show that a second synchrotron component is the only likely scenario left to explain the X-rays in these jets. Secondly, we find that irrespective of the X-ray emission mechanism, the deep upper limits at GeV energies place interesting constraints on the Doppler beaming factors which implies that these jets are not highly relativistic on the kpc scale. We will discuss the surprising implications of slow, synchrotron X-ray jets on our understanding of the total radiative output of quasars, especially at TeV energies.

1. methods

1.1. The *Fermi* Test of IC/CMB

As first noted by G06, the shape of the IC/CMB spectrum is constrained to match the synchrotron spectrum, with a shift in frequency and luminosity solely determined by the factor B/δ where δ is the Doppler beaming factor and B the magnetic field strength. From G06, we have:

$$\frac{\nu_c}{\nu_s} = \frac{\nu_{\text{CMB}} \delta^2 \gamma^2}{e B \delta \gamma^2 / [2\pi m_e c (1+z)]} \quad (1)$$

$$\frac{L_c}{L_s} = \frac{32\pi U_{\text{CMB}} (1+z)^4 \delta^4}{3(B\delta)^2}, \quad (2)$$

where ν_c and ν_s (L_c , L_s) are the observed Compton and synchrotron frequencies (luminosities) emitted by electrons of Lorentz factor γ , e and m_e are the electron charge and mass, and $\nu_{\text{CMB}} = 1.6 \times 10^{11}$ Hz is the CMB peak frequency at $z = 0$. However, if the observed X-ray fluxes are to be produced by the IC/CMB mechanism, then the value of B/δ is already uniquely determined by the requirement to match the X-ray flux level, at which point there is no freedom at all in the rest of the spectrum. The peak of the IC/CMB spectrum will fall in the GeV band. Note that this prediction is not predicated on any particular (e.g., equipartition) magnetic field strength.

The *Fermi*/LAT lacks the spatial resolution to detect the jet separately from the gamma-ray bright quasar core, which is only $10''$ away – the *Fermi*/LAT 68% containment radius is on the order of tenths of a degree to degrees. However, in powerful quasars the inverse Compton core emission generally peaks at a few MeV, producing a soft, and extremely variable spectrum in the *Fermi* band, with long periods of relative quiescence. Indeed, PKS 0637-752 was detected in the 2nd *Fermi* source catalog [2FGL, Nolan et al. 2012] as both a very soft (photon index of $\Gamma_p = 2.71$)

and highly variable source (variability index = 347). In contrast, the IC/CMB emission from the large scale jet is expected to be harder and completely non-variable. The latter property allows us to combine the *Fermi* data taken only when the quasar core is in a low state to try to detect or place limits on the IC/CMB emission.

1.2. Fermi Analysis of PKS 0637-752

We first combined the all-sky weekly LAT event and spacecraft files for weeks 9 through 325 of the *Fermi* mission, corresponding to Fermi Mission Elapsed Time (MET) from 239557417 to 430608212 and calendar dates 4 August 2008 to 24 August 2014. In order to analyze the region around PKS 0637-752, we used the publicly available ‘quickAnalysis’ script. The public scripts mentioned here are available at <http://fermi.gsfc.nasa.gov/ssc/data/analysis/user/> to run the *Fermi* analysis tools and generate the filtered event file, livetime cube, and exposure map, using a region of interest (ROI) of 10° and an otherwise default configuration. The starting source list was generated from the publicly available make2FGLxml script, which generates the xml file pre-populated with 2FGL catalog sources. We used a binned maximum Likelihood to get an initial fit for all the catalog sources in our ROI. We also included sources a further 5° out from our ROI, but always fixed to the catalog values. PKS 0637-752 was detected with a very high test-statistic (TS, roughly significance squared) value of 289, a 100 MeV to 100 GeV photon flux of $3.16 \times 10^{-8} \text{ s}^{-1} \text{ cm}^{-2}$, and a photon index $\Gamma_p = 2.64$, similar to the value reported in the 2FGL catalog.

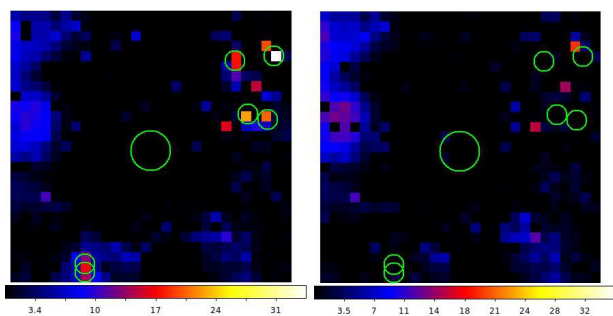


Figure 2: *Left*: An initial TS map of the region around PKS 0637-752, showing the excess TS present in 0.5° pixels over the best-fit likelihood model using 2FGL catalog sources. The large circle marks the position of PKS 0637-752. The smaller circles mark the positions of the six new sources not present in the 2FGL catalog (corresponding to regions of excess TS with pixel values >20). *Right*: The updated TS map (same FOV and binning) after the six sources were localized and fit with a binned likelihood.

Table I New sources in ROI of Targets

0637-752			3C 273		
RA _{2k}	Dec _{2k}	TS	RA	Dec	TS
(deg)	(deg)		(deg)	(deg)	
82.43046	-72.74572	57.5	192.82676	-2.00263	70.7
81.13040	-69.60575	60.5	190.96827	-2.29561	82.3
78.98804	-72.72570	28.6	187.15935	-3.29476	60.2
86.33797	-70.34640	39.6	184.47577	-0.48239	92.5
119.70430	-80.70430	9.9	193.43690	3.47391	224.6
118.83300	-80.32970	16.1	192.63313	2.25116	65.7

We checked for additional significant sources within 7° of PKS 0637-752 but not in the 2-year LAT catalog by making a TS residual map. Rough starting positions of apparent new significant sources were measured from the TS map by hand, only considering as candidates those with a central pixel value (TS) > 20 . Each new source was added to the XML model file as a powerlaw, and an initial spectral parameter fit derived via binned likelihood. We then refined the position of each source one at a time while the spectral parameters were held fixed. The existing tool, `gtfindsrc`, only works for unbinned likelihood analysis, so we built our own binned version of the tool which works in the same way. Using the frozen model, we used the python `minimize` function in the `scipy` package (L-BFGS-B method) to optimize the log-likelihood value versus the RA and Dec position, given a reasonable range of about 1 degree around the starting positions noted by hand. For the 7° ROI around PKS 0637-752, six new sources were added to the model, and an updated TS map run from this larger source list shows that the excess TS previously seen is now gone (right panel of Figure 2). A list of the new sources with their location and TS value is given at left in Table I.

PKS 0637-752 is a significant *Fermi* source, and was detected in the 2nd *Fermi* catalog, as 2FGL J0635.5-7516. Our approach to detecting and/or setting limits on the IC/CMB gamma-ray emission exploits the variability of the blazar core which cannot be spatially resolved separately from the large-scale jet due to the poor angular resolution of *Fermi*. During times when the blazar is quiescent, the hard, steady emission from IC/CMB will either appear as a steady plateau, or else the upper limits generated will place constraints on the level of the IC/CMB emission. In order to build a lightcurve of the core, the full 6-year dataset is divided into bins of equal good time interval (GTI) time, totalling 10.5 days. We then used our updated (2FGL + 6 new) model described above and ran a binned likelihood to fit PKS 0637-752 as a power-law source, with sources more than 5° away fixed. The resulting lightcurve for the core over the full time range is shown in Figure 3, with the 100 MeV - 100 GeV photon flux shown on top and the corresponding TS shown below. The clear variability in the light curve indicates that the total *Fermi* flux is dominated by

the core.

We next began a ‘progressive binning’ analysis, in which the lightcurve bins were ordered from lowest to

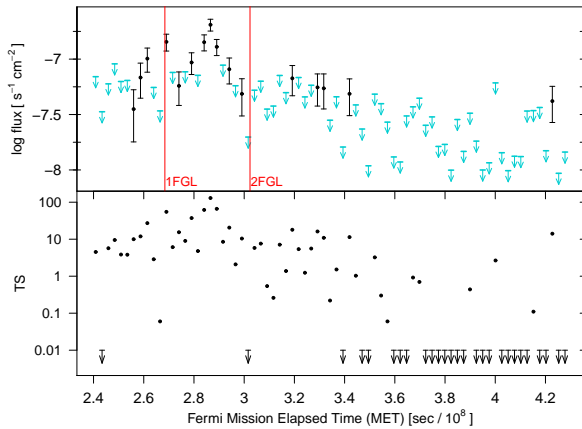


Figure 3: *Upper*: Lightcurve of PKS 0637-752. The total 100 MeV - 100 GeV photon flux for PKS 0637-752 in 10.5-day (total GTI) bins versus the mean Mission Elapsed Time (MET) of the bin. Upper limits are shown where $TS < 10$. The red verticle lines show the end-time for the 1FGL and 2FGL catalogs. *Lower*: The TS value corresponding to the same bin as above.

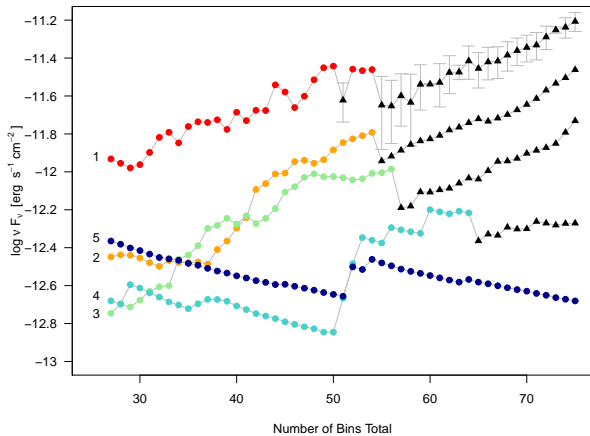


Figure 4: The results of the progressive binning analysis on PKS 0637-752. The upper axis gives the νF_ν flux while lower axis gives the total number of bins combined (where ordering is based on TS value and not time order), starting from the 27 bins with $TS < 0.01$. The points give the upper limits (colored dots) or detected fluxes ($TS > 10$, black triangles) for each of the five *Fermi* energy bands (red, orange, green, cyan, navy from lowest to highest energy). Errors on the detected fluxes are only shown for the lowest-energy bin for clarity but are similar across bins. For the highest-energy bin (10 - 100 GeV) no detection is ever made. The increasing fluxes indicate that the quasar core is being detected in the other bands.

highest TS value. Of the entire set of 75 time bins, 27 showed a TS level consistent with zero for the location of PKS 0637-752 (upper limits in lower panel of Figure 3). Starting from these 27 bins combined, we progressively combine the event files for the lowest bins plus the next lowest bin in TS, at each step optimizing the fit of PKS 0637-752 and the sources within 5° with a binned likelihood. We repeated adding the next-highest bin and getting the maximum likelihood fit until all bins had been added together. Note that this re-combining of the lightcurve in a discontinuous way is appropriate for deriving a limit on the large-scale jet because the IC/CMB emission is predicted to be completely non-variable, and thus there is no risk of any selection effect via variability. The variable core clearly dominates the flux levels determining the ordering, and is disconnected from the jet in any case. At each step we evaluated the TS and flux level in the five canonical *Fermi* energy bands of 0.1-0.3, 0.3-1, 1-3, 3-10 and 10-100 GeV, calculating the 95% upper limit flux value when $TS < 10$ in any given bin. Previous work on 3C 273 has shown that the exact ordering of the bins (whether by using the TS value or the total flux or upper limit value for the bin) does not significantly affect the resulting upper limits (M14).

As shown in Figure 4, the highest energy bands gave upper limits which decreased with the increasing exposure as more bins are added, where we have color-coded the upper limits in the 5 energy bands, and black triangles indicate a significant detection in the band. The decrease in upper limits sometimes going faster than $1/\sqrt{t}$ and ‘jumpy’ behavior is expected in the case of very low backgrounds and low count rates. Note that in the lower-energy bins, where the PKS 0637-752 quasar core dominates due to its soft spectrum, the upper limits reach a minimum rather quickly, and generally increase before becoming detections. It must be noted that the detected *Fermi* emission in these bands is from the quasar core, not the large-scale jet, based on the soft spectrum, and the fact that the emission level rises as more bins are added (showing that the source is indeed variable and that the bins are ordered by flux level). While the 4th energy band detected points do not rise as quickly as the first three, the flux level is far above the upper limit derived after 50 bins, so cannot be the steady emission of the large-scale jet, which must be below this limit. The highest bin never shows a significant detection of either component.

1.3. *Fermi* Analysis of 3C 273

We re-analyzed the *Fermi* data for 3C 273 using the 6-year dataset to compare with the results from M14 using 4.5 years of data, as the core remained relatively quiescent over the additional time elapsed. We followed the same procedure as outlined above for

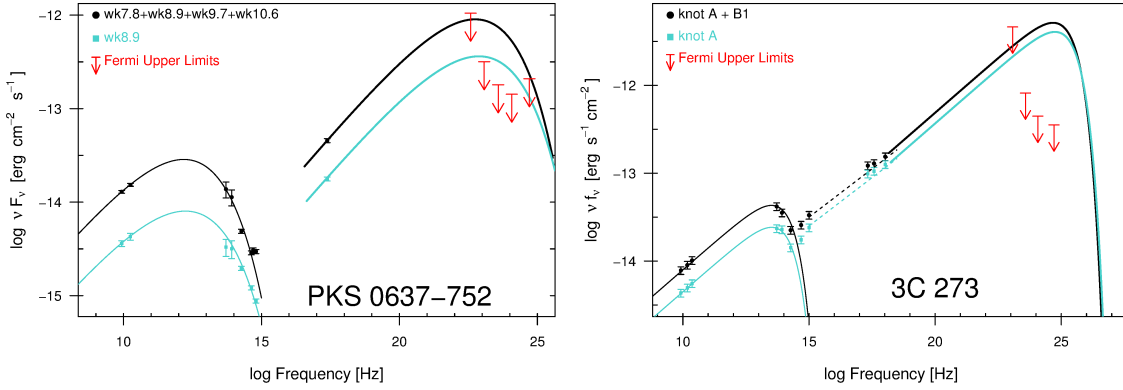


Figure 5: *Left*: The SED for the large-scale jet of PKS 0637-752. Data for the four brightest X-ray detected knots combined is shown as black points. The SED of the X-ray brightest knot, wk8.9, is plotted with blue points. *Right*: The SED for the knots of 3C 273, with black points for knots A and B1 combined, and blue for X-ray brightest knot A only. For both plots, the *Fermi* 95% upper limits are shown in red.

PKS 0637-752, finding six new sources within 7° of the position of 3C 273, listed at right in Table I. The core of 3C 273 was detected with a TS of 17504, with a 100 MeV - 100 GeV photon flux of $3.68 \times 10^{-7} \text{ s}^{-1} \text{ cm}^{-2}$ and $\Gamma_p = 2.67$. A lightcurve was made using bins totaling 10.5 days in GTI time, and ordered according to TS (a total of 88 bins). The progressive-binning was started from the single lowest bin, with the next-highest bin continually added as described above until all bins were added. At each step the flux (or 95% upper limit) was calculated for the five canonical *Fermi* energy bins.

2. Results: Testing the IC/CMB Model

We show in Figure 5 the radio to X-ray SEDs for the jet of both PKS 0637-752 (left) and 3C 273 (right). For PKS 0637-752 we have taken both the *Chandra* X-ray and Hubble Space Telescope (HST) infrared and optical data (NICMOS, WFPC2 and ACS) from Mehta et al. [2009]. We have also re-derived the *Spitzer* infrared fluxes for the brightest complex of knots (wk7.8, wk8.9, wk9.7, wk10.7), following the same methods reported in Uchiyama et al. [2005]. We have also measured updated radio fluxes based on a re-analysis of archival and new ATCA data at 4.8, 8.4, and 17.8 GHz. For 3C 273, data is taken from Jester et al. [2006, 2005] and Uchiyama et al. [2006] and references therein.

In both figures, we consider two scenarios: the first combines the photometry of the brightest/nearest knots to the core in order to test the IC/CMB prediction (black points and lines). In 3C 273, Jester et al. [2005] have already shown that only knots A and B1 have X-ray indices similar to their radio indices (which is required for IC/CMB), so our “combined

knot” scenario includes only these two knots. For PKS 0637-752, we use all the bright X-ray knots just before the turn in the jet (wk7.8, wk8.9, wk9.7, and wk10.6) where one might assume that some deceleration likely takes place. The second scenario assumes that the X-rays from the weaker knots are already *not* from IC/CMB, and so only the photometry of the X-ray brightest knot is plotted (knot A in 3C 273 and wk8.9 in PKS 0637-752, plotted as blue points and lines). The thin solid lines through radio-optical points show a (phenomenological) synchrotron spectrum fitting the data, while the heavy line shows the corresponding IC/CMB curve to match the X-ray flux levels. As shown, for both jets, the 95% upper limits in several bands violate the IC/CMB predictions under either scenario.

We report in the upper part of Table II a summary of the *Fermi* data analysis for PKS 0637-752 and 3C 273. We list the definition of the energy bins in columns 2-5, followed by the deepest 95% upper limit flux level (in νF_ν) reached in our progressive binning for each energy bin in column 6. The corresponding number of bins co-added is given in column 7. In column 8 we list the flux predicted under the IC/CMB at the frequency given in column 5. This flux corresponds to the IC/CMB model prediction for the combination of knots wk7.8, wk8.9, wk9.7, and wk10.7 in PKS 0637-752, and knots A and B1 for 3C 273. In the former case, we do not include the only other X-ray detected not (wk5.7) because it is not consistently detected at other wavelengths. For 3C 273, only knots A and B1 have X-ray spectra consistent with their radio spectra, so the knots further downstream are assumed to be producing X-rays via synchrotron emission. In column 10, we have calculated at what significance level our observations rule out the level of predicted IC/CMB flux given in col-

Table II Results of the Fermi Data Analysis

Source	Band	E_1 (GeV)	E_2 (GeV)	log Freq. (Hz)	95% Limit ($\text{erg s}^{-1} \text{cm}^{-2}$)	Bins Added	Combined Knots ^{a*} $F_{\text{IC/CMB}}$ ($\text{erg s}^{-1} \text{cm}^{-2}$)	% Ruled Out	Single Knot ^{b†} $F_{\text{IC/CMB}}$ ($\text{erg s}^{-1} \text{cm}^{-2}$)	% Ruled Out
(1)	(2)	(3)	(4)	(5)	(6)	(7)	(8)	(9)	(10)	(11)
0637-752	1	0.1	0.3	22.6	1.05×10^{-12}	29	9.0×10^{-13}	92.9	3.6×10^{-13}	...
	2	0.3	1	23.1	3.17×10^{-13}	32	8.8×10^{-13}	99.8	3.6×10^{-13}	94.5
	3	1	3	23.6	1.80×10^{-13}	27	7.4×10^{-13}	99.98	3.2×10^{-13}	98.7
	4	3	10	24.1	1.43×10^{-13}	50	5.3×10^{-13}	99.95	2.5×10^{-13}	98.6
	5	10	100	24.7	2.09×10^{-13}	75	2.3×10^{-13}	95.9	1.3×10^{-13}	...
3C 273	1	0.1	0.3	22.6	2.72×10^{-11}	1	2.1×10^{-12}	...	1.6×10^{-12}	...
	2	0.3	1	23.1	4.63×10^{-12}	2	2.8×10^{-12}	...	2.1×10^{-12}	...
	3	1	3	23.6	8.20×10^{-13}	5	3.6×10^{-12}	>99.99	2.8×10^{-12}	>99.99
	4	3	10	24.1	4.46×10^{-13}	31	4.5×10^{-12}	>99.99	3.5×10^{-12}	>99.99
	5	10	100	24.7	3.56×10^{-13}	30	5.2×10^{-12}	>99.99	4.1×10^{-12}	>99.99

umn 9. For the final two columns, we also give the predicted flux under IC/CMB and the significance-level that we can rule it out, but only for the X-ray brightest knot of each jet (wk8.9 and knot A, respectively). As shown, the IC/CMB model is ruled out at a $> 99.9\%$ level for PKS 0637-752 and at $> 99.99\%$ level for 3C 273.

3. Discussion

These two cases where the IC/CMB origin for the X-rays has been unambiguously ruled out join with that of PKS 1136-135, where high UV polarization has shown that the second component (UV to X-ray) must be synchrotron in origin, since significant polarization is not expected in the IC/CMB scenario [Cara et al. 2013]. we focus the rest of the paper on the implications for jet physics if the X-ray flux in quasar jets is synchrotron emission from a separate, high-energy electron population.

A synchrotron origin for the X-rays is not in conflict with any of the data in hand, and further, relaxes many of the ‘uncomfortable’ constraints of the IC/CMB model. Very small angles to the line of sight are not required, and the total jet power required is considerably less [Dermer and Atoyan 2004], as the electron energy distribution need not be extended to very low values. The main objection to a second component heretofore has simply been its unexplained nature; Schwartz et al. [2000] notes that there is no reason why a second population of high-energy electrons should be co-spatial with the first. However, this co-occurrence of two very different electron populations, if the correct interpretation, is obviously a very important clue to the particle acceleration mechanism in large-scale jets, of which we still know little.

An interesting consequence follows for our accounting of the large-scale-jet contribution to various backgrounds, especially at TeV energies. Jet one-sidedness

clearly indicates that the kpc-scale jets are at least mildly relativistic, and thus IC/CMB emission must occur at some level. Due to the very low background in the highest-energy *Fermi* bands, the flux limits reachable by *Fermi*’s sky-scanning mode of operation should allow us to eventually either detect this emission or put very strong limits on the factor of B/δ which characterizes the flow on the kpc scale. The current *Fermi* upper limits already constrain $\delta \lesssim 7.8$ for 3C 273 and $\delta \lesssim 6.5$ for PKS 0637-752, under the assumption of equipartition magnetic fields, where we take $B\delta = 1.5 \times 10^{-5}$ G for PKS 0637-752 from Tavecchio et al. [2000] and $B\delta = 1.0 \times 10^{-4}$ for 3C 273 from G06. These limits are already low enough to have interesting consequences for our understanding of the total radiative output of AGN jets on the kpc scale.

It is generally assumed that the radiative output of quasar jets is dominated by that occurring at the ‘core’, the base of the jet which is presumed to be very near the black hole (or \sim parsecs away at most) and is therefore unresolved even in VLBI imaging. Certainly, the observed fluxes are dominated by this part of the jet due to Doppler beaming whenever the jet is pointed fairly along our line-of-sight. This is depicted in Figure 6, where the core points of both jets are shown as gray circles, and the jet photometry as gray triangles (flux scale on right axis). The luminosity scale at left applies to these points only under the incorrect assumption of isotropy. If we correct these values for beaming, we get the real ‘angle-integrated’ total power output from the core and the jet, plotted as a dark blue dashed line and the gray shaded area, respectively. VLBI observations of superluminal motions place a lower limit on $\Gamma=15$ for the cores of both 3C 273 and PKS 0637-752, respectively [Lister et al. 2013, Edwards et al. 2006]. We have applied a correction (multiplying by $1/\delta^2$) assuming $\delta=15$ for the cores of both jets to give the angle-integrated core luminosity (dark blue dashed line). To calculate the angle-integrated luminosity of

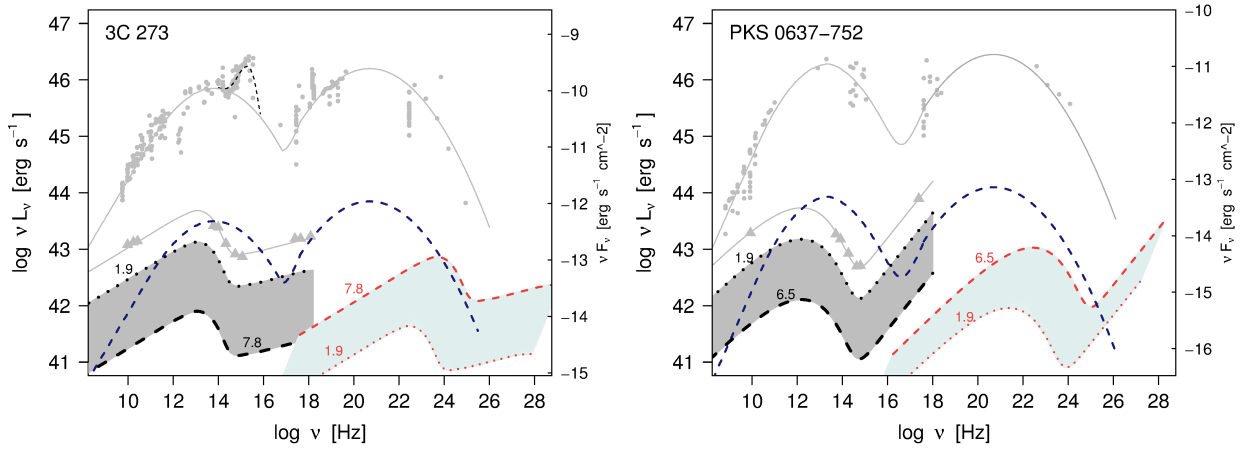


Figure 6: (Note: Figure description below applies to both panels; 3C 273 is shown at left and PKS 0637-752 is shown at right). The Core flux points are shown as gray circles with phenomenological SED fit through the points as a thin gray line (big blue bump shown as black dashed line and not included in the beamed emission fits). In comparison, the core points are shown as gray triangles. The flux scale at right only applies to solid curves in the figure. The impression of the total dominance of the core flux is mainly a product of the beaming difference between the two components, as seen when beaming-corrected (angle-integrated) luminosities are plotted, rather than those assuming isotropy. Blue dashed line is the core fit times $1/\delta^2$ with $\delta = 15$ for both jets. The gray zone is the range of possible beaming-corrected SEDs for the knots given our current constraints on δ for the knots. Finally, the light blue shaded area is the range of IC/CMB emission possible given the same δ constraints. Note that the TeV emission in particular is already constrained to be much higher than is typical for ‘TeV blazars’ ($\approx 10^{41}$ erg s $^{-1}$).

the knots, we apply a lower limit value of $\delta = 1.9$ which comes from statistical arguments based on populations [Arshakian and Longair 2004], which gives the dotted-line upper edge to the gray shaded area, while the current δ limits from *Fermi* give the lower dashed-line limit. The true angle-integrated luminosity of the knots is thus somewhere in the gray zone.

It is interesting to note that the knots are apparently *not* insignificant in total output when compared to the core. Definite conclusions will require tighter constraints on the δ factors of both the core and the knots, but it is possible that large-scale jets contribute more than the core in the UV to X-rays, in addition to their general dominance in the radio (which was already well known). Large-scale jets could thus be an important contributor to some astrophysical backgrounds.

A further observation follows from the realization that the X-rays are synchrotron in origin: the electrons producing the synchrotron X-rays will themselves upscatter the CMB to produce a GeV to TeV spectrum. The angle-integrated total power in the IC/CMB component is shown in Figure 6 as a light blue shaded area. Note that the bounds in this case are flipped; the upper δ limit forms the upper edge of the allowed zone. Even in the minimum $\delta=1.9$ case, these jets are already constrained to produce fluxes in excess of 10^{41} erg s $^{-1}$ which is the typical total radiative output for the canonical low-power FR I type ‘TeV blazars’. We have not applied an EBL correction to these spectra merely to illustrate the total intrinsic

output. However, EBL absorption is very important at TeV energies, and would make direct observation of this TeV component very difficult. Even assuming the most optimistic case of $\delta=7.8$ for 3C 273, at redshift 0.158 the EBL absorption [Finke et al. 2010] is already high enough that it would take at least 100 hours of observations by the future CTA mission to detect the beamed IC/CMB component at TeV energies. Thus it is unlikely that many anomalous X-ray jets will have a synchrotron origin for the X-rays directly confirmed via TeV observations, though if *Fermi* begins detecting the IC/CMB component, an upturn at the highest energies might be visible in a few cases. The remaining best direct observation is via polarization – either in the UV, for those that show the second component emerging there, or with future X-ray polarimeters. Finally, we note that as long as *Fermi* continues to operate, the low background at the highest energies should allow continually improving constraints on the δ factors of large-scale jets.

Acknowledgments

Work supported by Fermi Grant NNX13AO88G.

References

- D. A. Schwartz, H. L. Marshall, J. E. J. Lovell, B. G. Piner, S. J. Tingay, M. Birkinshaw, G. Chartas, M. Elvis, E. D. Feigelson, K. K. Ghosh, et al., *ApJ* **540**, L69 (2000), astro-ph/0005255.
- G. Chartas, D. M. Worrall, M. Birkinshaw, M. Cresitello-Dittmar, W. Cui, K. K. Ghosh, D. E. Harris, E. J. Hooper, D. L. Jauncey, D.-W. Kim, et al., *ApJ* **542**, 655 (2000), astro-ph/0005227.
- A. S. Wilson and Y. Yang, *ApJ* **568**, 133 (2002), astro-ph/0112097.
- S. G. Jorstad, A. P. Marscher, M. L. Lister, A. M. Stirling, T. V. Cawthorne, W. K. Gear, J. L. Gómez, J. A. Stevens, P. S. Smith, J. R. Forster, et al., *AJ* **130**, 1418 (2005), astro-ph/0502501.
- M. L. Lister, M. H. Cohen, D. C. Homan, M. Kadler, K. I. Kellermann, Y. Y. Kovalev, E. Ros, T. Savolainen, and J. A. Zensus, *AJ* **138**, 1874 (2009), 0909.5100.
- T. G. Arshakian and M. S. Longair, *MNRAS* **351**, 727 (2004), astro-ph/0310503.
- L. M. Mullin and M. J. Hardcastle, *MNRAS* **398**, 1989 (2009), 0906.2088.
- F. Tavecchio, L. Maraschi, R. M. Sambruna, and C. M. Urry, *ApJ* **544**, L23 (2000), astro-ph/0007441.
- A. Celotti, G. Ghisellini, and M. Chiaberge, *MNRAS* **321**, L1 (2001), astro-ph/0008021.
- R. M. Sambruna, C. M. Urry, F. Tavecchio, L. Maraschi, R. Scarpa, G. Chartas, and T. Muxlow, *ApJ* **549**, L161 (2001), astro-ph/0101299.
- R. M. Sambruna, L. Maraschi, F. Tavecchio, C. M. Urry, C. C. Cheung, G. Chartas, R. Scarpa, and J. K. Gambill, *ApJ* **571**, 206 (2002), astro-ph/0201412.
- A. Siemiginowska, R. K. Smith, T. L. Aldcroft, D. A. Schwartz, F. Paerels, and A. O. Petric, *ApJ* **598**, L15 (2003), astro-ph/0310241.
- R. M. Sambruna, J. K. Gambill, L. Maraschi, F. Tavecchio, R. Cerutti, C. C. Cheung, C. M. Urry, and G. Chartas, *ApJ* **608**, 698 (2004), astro-ph/0401475.
- H. L. Marshall, D. A. Schwartz, J. E. J. Lovell, D. W. Murphy, D. M. Worrall, M. Birkinshaw, J. M. Gelbord, E. S. Perlman, and D. L. Jauncey, *ApJS* **156**, 13 (2005), astro-ph/0409566.
- D. E. Harris and H. Krawczynski, *ARA&A* **44**, 463 (2006), astro-ph/0607228.
- A. Siemiginowska, L. Stawarz, C. C. Cheung, D. E. Harris, M. Sikora, T. L. Aldcroft, and J. Bechtold, *ApJ* **657**, 145 (2007), astro-ph/0611406.
- H. L. Marshall, J. M. Gelbord, D. A. Schwartz, D. W. Murphy, J. E. J. Lovell, D. M. Worrall, M. Birkinshaw, E. S. Perlman, L. Godfrey, and D. L. Jauncey, *ApJS* **193**, 15 (2011), 1101.5822.
- P. Kharb, M. L. Lister, H. L. Marshall, and B. S. Hogan, *ApJ* **748**, 81 (2012), 1201.4178.
- L. E. H. Godfrey, G. V. Bicknell, J. E. J. Lovell, D. L. Jauncey, J. Gelbord, D. A. Schwartz, E. S. Perlman, H. L. Marshall, M. Birkinshaw, D. M. Worrall, et al., *ApJ* **755**, 174 (2012), 1208.0069.
- M. J. Hardcastle, *MNRAS* **366**, 1465 (2006), astro-ph/0511511.
- C. D. Dermer and A. Atoyan, *ApJ* **611**, L9 (2004), astro-ph/0404139.
- Y. Uchiyama, C. M. Urry, C. C. Cheung, S. Jester, J. Van Duyne, P. Coppi, R. M. Sambruna, T. Takahashi, F. Tavecchio, and L. Maraschi, *ApJ* **648**, 910 (2006), astro-ph/0605530.
- S. Jester, D. E. Harris, H. L. Marshall, and K. Meisenheimer, *ApJ* **648**, 900 (2006), astro-ph/0605529.
- D. E. Harris, A. E. Mossman, and R. C. Walker, *ApJ* **615**, 161 (2004), astro-ph/0407354.
- J. Kataoka and L. Stawarz, *ApJ* **622**, 797 (2005), astro-ph/0411042.
- M. Cara, E. S. Perlman, Y. Uchiyama, C. C. Cheung, P. S. Coppi, M. Georganopoulos, D. M. Worrall, M. Birkinshaw, W. B. Sparks, H. L. Marshall, et al., *ApJ* **773**, 186 (2013), 1305.2535.
- M. Georganopoulos, E. S. Perlman, D. Kazanas, and J. McEnery, *ApJ* **653**, L5 (2006), astro-ph/0610847.
- E. T. Meyer and M. Georganopoulos, *ApJ* **780**, L27 (2014), 1307.8421.
- P. L. Nolan, A. A. Abdo, M. Ackermann, M. Ajello, A. Allafort, E. Antolini, W. B. Atwood, M. Axelsson, L. Baldini, J. Ballet, et al., *ApJS* **199**, 31 (2012), 1108.1435.
- K. T. Mehta, M. Georganopoulos, E. S. Perlman, C. A. Padgett, and G. Chartas, *ApJ* **690**, 1706 (2009), 0809.1608.
- Y. Uchiyama, C. M. Urry, J. Van Duyne, C. C. Cheung, R. M. Sambruna, T. Takahashi, F. Tavecchio, and L. Maraschi, *ApJ* **631**, L113 (2005), astro-ph/0508569.
- S. Jester, H.-J. Röser, K. Meisenheimer, and R. Perley, *A&A* **431**, 477 (2005), astro-ph/0410520.
- M. L. Lister, M. F. Aller, H. D. Aller, D. C. Homan, K. I. Kellermann, Y. Y. Kovalev, A. B. Pushkarev, J. L. Richards, E. Ros, and T. Savolainen, *AJ* **146**, 120 (2013), 1308.2713.
- P. G. Edwards, B. G. Piner, S. J. Tingay, J. E. J. Lovell, J. Kataoka, R. Ojha, and Y. Murata, *PASJ* **58**, 233 (2006).
- J. D. Finke, S. Razzaque, and C. D. Dermer, *ApJ* **712**, 238 (2010), 0905.1115.